THE JOURNAL OF PHYSICAL CHEMISTRY B

pubs.acs.org/JPCB

Article

Macromolecular Crowding: How Shape and Interactions Affect Diffusion

Tomasz Skóra, Farzaneh Vaghefikia, Jörg Fitter,* and Svyatoslav Kondrat*

Cite This: J. Phys. Chem. B 2020, 124, 7537−7543

Read Online

ACCESS | Metrics & More | Article Recommendations | Supporting Information

ABSTRACT: A significant fraction of the cell volume is occupied by various proteins, polysaccharides, nucleic acids, etc., which considerably reduces the mobility of macromolecules. Theoretical and experimental work so far have mainly focused on the dependence of the mobility on the occupied volume, while the effect of a macromolecular shape received less attention. Herein, using fluorescence correlation spectroscopy (FCS) and Brownian dynamics (BD) simulations, we report on a dramatic slowdown of tracer diffusion by cylindrically shaped double-stranded (ds) DNAs (16 nm in length). We find, for instance, that the translational diffusion coefficient of a streptavidin tracer is reduced by about 60% for a volume fraction of dsDNA as low as just 5%. For comparison, for a spherical crowder (Ficoll70) the slowdown is only 10% at the same volume fraction and 60% reduction occurs at a volume fraction as high as 35%. BD simulations reveal that this reduction can be attributed to a larger volume excluded to a tracer by dsDNA particles, as compared with spherical Ficoll70 at the same volume fraction, and to the differences in the tracer−crowder attractive interactions. In addition, we find using BD simulations that rotational diffusion of dsDNA is less affected by the crowder shape than its translational motion. Our results show that diffusion in crowded systems is determined not merely by the occupied volume fraction, but that the shape and interactions can determine diffusion, which is relevant to the diverse intracellular environments inside living cells.

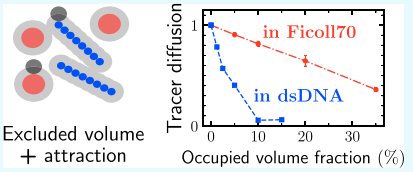

INTRODUCTION

Up to 40% of the cell volume is occupied by macromolecules.[1,2] Such macromolecular crowding affects protein stability,[3] chemical equilibria,[4] gene regulation,[5] metabolic reactions,[6−8] and the diffusion of macromolecules.[9−17] Macromolecular diffusion plays an important role in various intracellular processes, such as metabolism, catalysis, signal transduction, transcription, and translation.[18,19] The theoretical and experimental work so far have focused on anomalous subdiffusion,[20−22] and on the role of interactions[23−25] and composition,[13,15,26−28] often using spherical crowders. However, the cell interior comprises macromolecules of various shapes and sizes.[29] Although some of them are globular (e.g., hemoglobin), the majority have diverse shapes, ranging from triangular (e.g., aspartate carbamoyltransferase), and Y and V-shapes (e.g., immunoglobulin and tRNA) to elongated cylindrical shapes (e.g., glucagon and tyrosyl-tRNA synthetase).

The previous work has indicated that shape anisotropy can cause transient (short-time) diffusion anisotropy[30] and contribute in a nonmonotonic way to short-time cage diffusion.[31] Shin et al. studied diffusion of star-like particles in crowded two-dimensional solutions and found nonmonotonic dependence of the translational diffusion on the strength of interactions.[32] Balbo et al. studied self-diffusion of Y-shaped γ-immunoglobulin (IgG) and smaller heart-shaped bovine serum albumin (BSA).[33] They found that IgG crowders reduced the tracer diffusion more strongly than BSAs. Significant deviations were observed at volume fractions of about 10% and higher, while the differences in the diffusion slowdown amounted to about 10−20%. However, since IgG and BSA have not only different shapes, but also different sizes, which additionally affects tracer diffusion,[27,34] the role played by the macromolecular shape cannot be straightforwardly singled out.

Herein, we use fluorescence correlation spectroscopy (FCS) and Brownian dynamics (BD) simulations to show that the shape- and interaction-induced slowdown of diffusion can be much stronger than the previously reported one. For crowders, we take spherical Ficoll70 (hydrodynamic radius 5.1 nm) and double-stranded (ds) DNA, which has a cylindrical shape with a diameter of about 2 nm and a sequence of 48 base pairs, resulting in a length of about 16 nm (hydrodynamic radius 3.9 nm, see Section S4 and Figure 1a). To our knowledge, this is the first time the dsDNA is used as a crowder. For a tracer, we take fluorescently labeled streptavidin, which is characterized by high structural stability, and for which no specific interactions with the above-mentioned crowders have been reported. To rationalize the experimental results, we perform BD simulations of systems akin to those studied by the FCS, and to identify the role of the shape, we simulate systems in which dsDNAs are

Received: May 29, 2020
Revised: August 3, 2020
Published: August 4, 2020

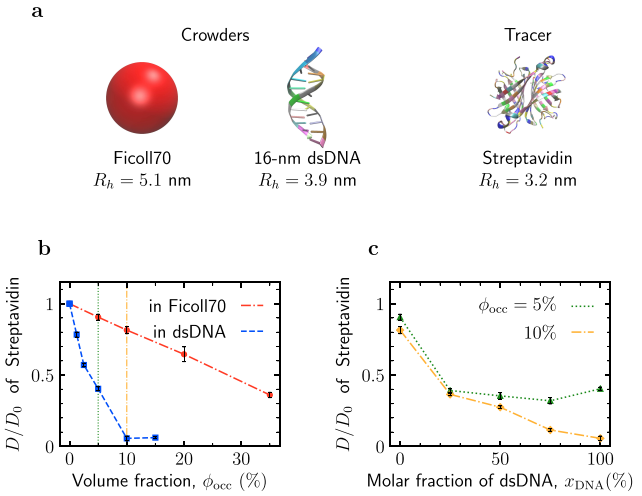

Figure 1. Effect of the macromolecular shape on diffusion from the FCS study. (a) Ficoll70 and double-stranded (ds) DNAs have been used as crowders and streptavidin as a tracer. Ficoll70 is a spherical macromolecule of a hydrodynamic radius of ≈5.1 nm. The length of dsDNA was ≈16 nm and the diameter was ≈2 nm; its hydrodynamic radius was measured by FCS and amounted to ≈3.9 nm. (b) Reduction of the diffusion coefficient D of streptavidin in Ficoll70 and in dsDNA as a function of the volume fraction ϕ_{occ} occupied by the respective crowders (spherical and cylindrical models have been used to calculate the volumes of Ficoll70 and dsDNA, respectively). D_0 is the diffusion coefficient of streptavidin in infinite dilution (no crowders). Thin vertical lines show volume fractions used in the panel (c). (c) Reduction of the diffusion coefficient D of streptavidin in a mixture of Ficoll70 and dsDNA as a function of the molar fraction x_{DNA} of dsDNA for two values of the occupied volume fraction ϕ_{occ}.

replaced by spherical particles with the same hydrodynamic radius as dsDNA.

METHODS

Fluorescence Correlation Spectroscopy (FCS) and Data Analysis. FCS measurements were performed with fluorescently labeled molecules freely diffusing in a solution on an inverted confocal microscope employing pulsed excitation and time-resolved photon detection (MicroTime 200, PicoQuant GmbH, Berlin, Germany). From data of the obtained time traces, intensity autocorrelation curves were calculated and analyzed using the SymPhoTime64 software (PicoQuant, Berlin, Germany). The autocorrelation curves were fitted with model functions for Brownian diffusion. The detailed description of the sample preparation, the microscope setup, the employed procedures for data treatment and analysis is given in Section S4. Examples of the fitted autocorrelation curves are shown in Figures S7 and S8.

Brownian Dynamics (BD) Simulations. We performed BD simulations with a customized version of the package BD_BOX.[35] We adopted the van der Waals interactions between particles to be appropriate for macromolecules[36,37] and likewise for electrostatic interactions for which we used the DLVO theory.[38] Long-range two-body hydrodynamic interactions were accounted for via the generalized Rotne−Prager−Yamakawa tensor[39−42] and Ewald summation was used to account for three-dimensional (3D) periodic boundary conditions. The positions of macromolecules were propagated with the Iniesta-de la Torre algorithm.[43] The box size was 75 nm × 75 nm × 75 nm. The temperature was 293.15 K and viscosity was tuned to reflect the water properties at that temperature (η = 1.005 cP). Simulation time was up to 20 μs with a time step of 0.5 ps. For details, see Section S1.

Monte Carlo (MC) Simulations. We performed MC simulations to compute volumes excluded to a tracer in Ficoll−dsDNA mixtures. Configurations were taken from BD simulations at various simulation times and for different initial conditions and served as an input for MC sampling. The excluded volumes were computed by sequentially inserting a tracer into these systems. The positions (and orientations, if any) of the inserted tracers were picked at random, assuming every position (and orientation) to be equally probable. In the case of Ficoll (dsDNA) as a tracer, one Ficoll (dsDNA) was first removed from the system before re-inserting it as a tracer. Excluded volume fractions were obtained by computing the ratio of the number of insertions, producing an overlap with any of the macromolecules present in the system, to the total number of insertions. For details, see Section S3A.

RESULTS AND DISCUSSION

Dramatic Slowdown of Diffusion by dsDNA Crowders. We first present the results of the FCS study. Figure 1b shows that already at an occupied volume fraction ϕ_{occ} as low as 5%, the diffusion of streptavidin was reduced by about 60%, as compared to the noncrowded system under the same conditions; for ϕ_{occ} above 10%, it was reduced to the values below the experimental accuracy. For comparison, the same figure shows the diffusion coefficient of streptavidin in a solution of spherical Ficoll70. The diffusion coefficient decreased linearly with ϕ_{occ} and achieved a reduction of about 60% for ϕ_{occ} = 35%. This is in agreement with previous work[10,16] but is in stark contrast with the diffusion in dsDNAs, where a comparable reduction in the diffusion coefficient was observed already at $\phi_{occ} \approx 5\%$.

We also measured the diffusion of streptavidin in a mixture of dsDNA and Ficoll70. Figure 1c shows that replacing Ficoll with dsDNAs reduces the streptavidin diffusion significantly. For the molar fraction of dsDNA x_{DNA} = 25%, the diffusion coefficient was about 60% of that observed without any crowder. Surprisingly, however, at this value of x_{DNA}, the diffusion was slowed down to approximately the same degree when the total occupied volume fraction was increased from ϕ_{occ} = 5% to ϕ_{occ} = 10%. Replacing Ficoll70 with dsDNAs further had a relatively moderate effect on the streptavidin diffusion (Figure 1c).

BD Simulations of Ficoll70−dsDNA Mixtures. To rationalize the FCS results, we performed Brownian dynamics (BD) simulations of the crowded systems similar to those studied by the FCS. We studied two-component systems containing spherical particles with the hydrodynamic radius of 5.1 nm, modeling Ficoll70, and particles consisting of eight connected spherical beads, each with the hydrodynamic radius of 1.14 nm, mimicking dsDNA (Figure 2a,c and Section S2). To single out the effect of shape, we considered only soft-core repulsive and hydrodynamic interactions between the macromolecules[24] and electrostatic repulsion between charged dsDNAs (Methods and Section S1).

The hydrodynamic radius of the model dsDNA was calculated from BD simulations of a single dsDNA by computing the mean-square displacement (MSD) of its center of mass $\mathbf{r}(t)$ (which is also its center of diffusion[44]), $\mathrm{MSD}(t) = \langle |\mathbf{r}(t) - \mathbf{r}(0)|^2 \rangle$, and fitting it to $\mathrm{MSD}(t) = 6D_0 t$ (Figure S2). The extracted diffusion coefficient was D_0 = 57.8 ± 1.4 nm^2 μs^{-1}, which gives a hydrodynamic radius of 3.70 ± 0.09 nm, matching the experimental value.

https://dx.doi.org/10.1021/acs.jpcb.0c04846
J. Phys. Chem. B 2020, 124, 7537−7543

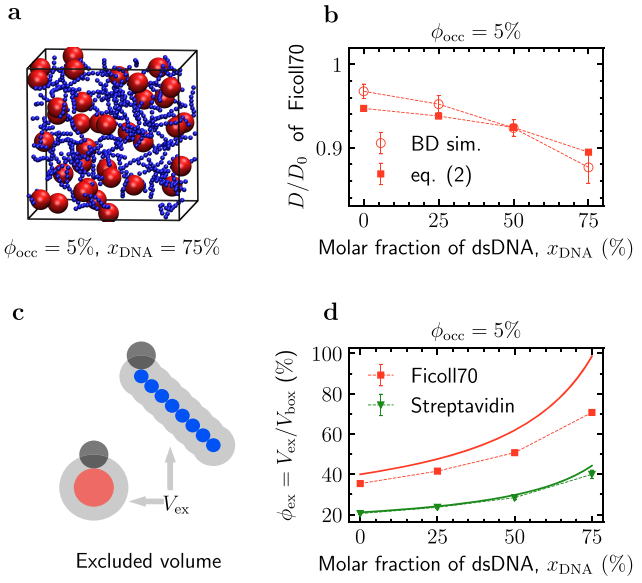

Figure 2. Effect of shape on macromolecular diffusion from BD simulations. (a) Snapshot from Brownian dynamics (BD) simulations of a mixture of spherical Ficoll70 (hydrodynamic radius 5.1 nm) and model dsDNA (8 beads of radius 1.14 nm). The hydrodynamic radius of dsDNA ≈3.7 nm, as obtained from 500 single-dsDNA BD simulations (Figure S2). (b) Reduction in the diffusion coefficient D of Ficoll70 as a function of the molar fraction of dsDNA, x_{DNA}, for a fixed occupied volume fraction $\phi_{occ} \approx 5\%$ (open circles). ϕ_{occ} for dsDNAs was calculated by summing up the bead volumes. D_0 is the diffusion coefficient of Ficoll70 without crowders. Filled squares show the result of fitting eq 2 to the BD data. In BD simulations, only steric, hydrodynamic, and electrostatic interactions were taken into account. (c) Volumes excluded to a tracer by Ficoll70 and by dsDNA. (d) Volume fractions $\phi_{ex} = V_{ex}/V_{box}$ excluded to Ficoll70 and to streptavidin in Ficoll70−dsDNA mixtures as functions of the molar fraction of dsDNA, x_{DNA}, for an occupied volume fraction $\phi_{occ} \approx 5\%$. V_{box} is the volume of a simulation box. The solid lines show eq 1, which does not take into account the overlaps of excluded volumes, and symbols show the results of Monte Carlo simulations (Section S3 and Figure S5).

In simulations of Ficoll70−dsDNA mixtures, we kept the total occupied volume fraction $\phi_{occ} \approx 5\%$ fixed and varied the molar fraction of dsDNA, x_{DNA} (Figure 2b and Table S2). Instead of adding a small amount of streptavidin to the mixture and observing its diffusion, as in the experiments, for computational efficiency, we studied diffusion of Ficoll70. To obtain the same statistics with streptavidin as with Ficoll70, for streptavidin concentrations as in the experiments (nanomolar regime) and with the computational resources available to us (Intel Xeon E5-2680 v3, 48 CPU/job, 480 CPU in total), we would have to run simulations for about 2 years consecutively. We therefore decided to treat Ficoll70 as a tracer in favor of investigating a larger number of systems.

Figure 2b shows that diffusion of Ficoll70 was slowed down with increasing x_{DNA}, but the magnitude of the slowdown was smaller than in the experiments (for streptavidin). Nevertheless, in the mixture with 75% of dsDNAs, the diffusion coefficient of Ficoll70 was reduced about 4 times more strongly than in the Ficoll70-only system at the same occupied volume fraction ϕ_{occ} = 5% (ca. 12.7% vs 3%, respectively).

Role of the Excluded Volume. To interpret these results, we computed volumes excluded to a tracer by Ficoll70 and by dsDNA (Figure 2c). Neglecting possible volume overlaps, one can find the excluded volume fraction as a function of the molar fraction of dsDNA (Section S3)

$$\phi_{ex}(x_{DNA}) = \phi_{occ} \frac{(1 - x_{DNA})V_{ex}^{F} + x_{DNA}V_{ex}^{DNA}}{(1 - x_{DNA})V_{occ}^{F} + x_{DNA}V_{occ}^{DNA}} \quad (1)$$

where V_{occ}^{α} and V_{ex}^{α} are volumes occupied and excluded to a tracer by the particle α (α = {F, DNA} for Ficoll70 and dsDNA). For Ficoll70 as a tracer, one has $V_{ex}^{F} = 8V_{occ}^{F}$. A dsDNA excludes (to a Ficoll70) a volume of $V_{ex}^{DNA} \approx 2625$ nm^3, which is about 81 times larger than its occupied volume $V_{occ}^{DNA} \approx 33$ nm^3. For a streptavidin tracer used in the experiments, one has $V_{ex}^{F} \approx 4.2\ V_{occ}^{F}$ and $V_{ex}^{DNA} \approx 33\ V_{occ}^{DNA}$.

According to eq 1, ϕ_{ex} increases with increasing x_{DNA} (solid lines in Figure 2d). For Ficoll70 as a tracer, ϕ_{ex} reaches values above 100%, which is because eq 1 does not take into account the overlaps of excluded volumes. To account for such overlaps, we performed Monte Carlo simulations, where we placed a tracer (either Ficoll70 or streptavidin) randomly into the configurations taken from the BD simulations (Section S3). The MC simulations reveal that eq 1 describes the excluded volumes remarkably well for straptavidin but less accurately for Ficoll70 (see Figure S5 for the tracer size dependence). This is because ϕ_{ex} attains higher values for Ficoll70 due to its bigger size, and hence the contribution from the overlaps of excluded volumes becomes more significant.

Diffusion of a macromolecule in a crowded environment can be viewed as diffusion of a point particle in the space accessible to the center of mass of the macromolecule. Within this simple picture, and at low volume fractions, the diffusion coefficient can be roughly approximated by[45,46]

$$D(\phi_{ex}) = D_0(1 - \alpha\phi_{ex}) \quad (2)$$

where α is a constant that, in principle, depends on the shape and orientation of crowders. Neglecting this dependence and using our MC results for ϕ_{ex} (x_{DNA}) (Figure 2d), we fitted eq 2 to the BD data. Figure 2b shows that eq 2 describes the diffusion slowdown qualitatively well but shows quantitative deviations. The deviations are likely because we ignored the α (x_{DNA}) dependence, and because ϕ_{ex} in our system varied between 35 and 71%, which is not at all small. In addition, the space excluded to Ficoll70 changes over time on the same time scale as the diffusion of Ficoll70, which is also not taken into account in eq 2.

Effect of Shape. To study more explicitly the effect of shape, we simulated a system in which dsDNA particles were replaced by spherical particles with the same hydrodynamic radius as dsDNA (dsDNA-S for brevity, Figure 3a). We prepared two systems in a computer with the same occupied volume fraction, ϕ_{occ} = 5%, containing either dsDNA or dsDNA-S mixed with Ficoll70 (25% molar fraction of Ficoll70 in each system; Figure 3b,c). From the trajectories of the BD simulations, we extracted the time-dependent diffusion coefficient of Ficoll70, $D(t)$ = MSD(t)/(6t), which is shown in Figure 3d. It shows that diffusion of Ficoll70 in the system with dsDNA was slowed down 3 times more strongly than in the system with spherical dsDNA-S (ca. 12 and 4%, respectively).

Interestingly, the diffusion coefficients of dsDNA and dsDNA-S differ less than the slowdown of tracer diffusion caused by them as crowders (compare Figure 3e and Figure 3d). To see how this relates to excluded volumes, we used MC simulations to calculate volumes excluded to a single dsDNA and to a dsDNA-S in typical configurations taken from the BD simulations (for dsDNA, we counted the excluded volume

https://dx.doi.org/10.1021/acs.jpcb.0c04846
J. Phys. Chem. B 2020, 124, 7537−7543

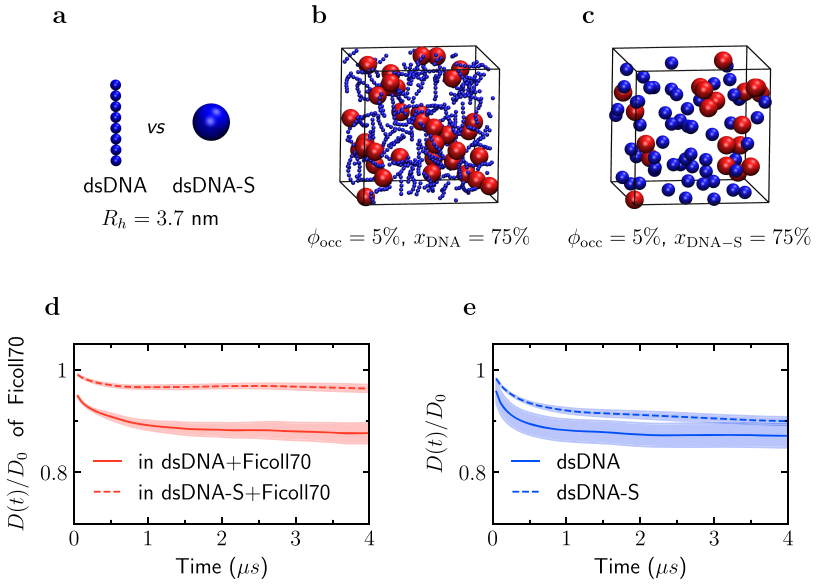

Figure 3. Spherical versus cylindrical macromolecules in BD simulations. (a) dsDNA particle is substituted with a spherical particle, dsDNA-S, of the same hydrodynamic radius as dsDNA. (b) Snapshot from BD simulations of a mixture of dsDNA and spherical Ficoll70 (hydrodynamic radius 5.1 nm). (c) Snapshot from BD simulations of a mixture of Ficoll70 and spherical dsDNA-S. (d) Diffusion coefficient $D(t)$ of Ficoll70 versus time in a mixture of Ficoll70 and dsDNA and in a mixture of Ficoll70 and dsDNA-S, as shown in panels (b) and (c). D_0 is the diffusion coefficient of Ficoll70 in infinite dilution in water (no crowders). The red shadowed areas show the uncertainties due to sampling errors. (e) Diffusion coefficients $D(t)$ of dsDNA and dsDNA-S versus time in systems in which they form mixtures with Ficoll70, as shown in panels (b) and (c). D_0 is the diffusion coefficient of dsDNA and dsDNA-S in water (no crowders). The blue shadowed areas show the uncertainties due to sampling errors accounted for the uncertainty in the dsDNA hydrodynamic radius.

proportionally to the spherical angle inaccessible to the dsDNA at a given position, see Section S3). We obtained 42 and 32% for dsDNA and dsDNA-S, respectively. The difference in the excluded volumes is much larger than the difference in the diffusion coefficients (about 1.5%, Figure 3e), highlighting that the excluded volume is unlikely the only factor affecting the slowdown of diffusion in crowded environments. The reason for these differences is, however, unclear.

Rotational Diffusion of dsDNA. The rotational diffusion coefficient D_r was computed by fitting mean orientation autocorrelations obtained from BD simulations to an exponentially decaying function of time (Section S1D2 and Figure S1). We first calculated the rotational diffusion coefficient in infinite dilution. Using 500 independent simulations of a single dsDNA, we obtained $D_{r,0} = 1.225 \pm 0.006$ rad^2 μs^{-1}.

To quantify how fast a dsDNA rotates, as compared to its translational motion, we introduced a parameter

$$k = \sqrt{\frac{2D_r}{3D_l}} \tag{3}$$

where D_l is the long-time translational diffusion constant, as before. Taking both diffusion constants in infinite dilution, we found $k \approx 6.8°$/nm. This means that a dsDNA rotates on average by 25° while traversing a distance equal to its hydrodynamic radius (≈3.7 nm) and by 124.5° for a distance equal to its length (≈18 nm), which takes ≈40 ns and 1 μs, respectively. Thus, rotations of dsDNA are relatively slow on the time scale of our simulations.

We next studied how rotational diffusion of dsDNA varies with its concentration, x_{DNA}, in a dsDNA−Ficoll70 mixture. Figure 4 demonstrates that D_r depends only weakly on x_{DNA} for ϕ_{occ} = 5%. For comparison, in the same figure we show the reduced translational diffusion coefficient D_l/D_0, which depends on x_{DNA} more significantly. Thus, unlike for translational diffusion, the volume fraction ϕ_{occ} = 5% was too low to reduce the rotational diffusion of dsDNA considerably. This is

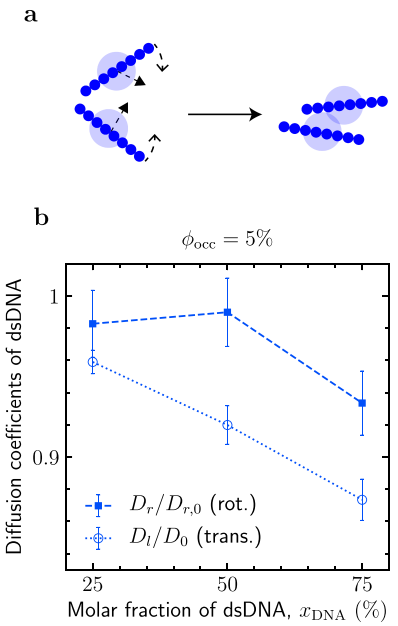

Figure 4. Rotational and translational diffusion of dsDNA from BD simulations. (a) Schematics of translational and rotational diffusion of dsDNA. The latter may be followed by tracing the orientation of a vector connecting the two most distant dsDNA beads. The shadowed areas show the hydrodynamic radius. (b) Rotational (D_r) and long-time translational (D_l) diffusion coefficients as functions of the molar fraction of dsDNA, x_{DNA}. Diffusion coefficients are expressed in terms of their values in infinite dilution, $D_{r,0}$ and D_0, respectively.

https://dx.doi.org/10.1021/acs.jpcb.0c04846
J. Phys. Chem. B 2020, 124, 7537−7543

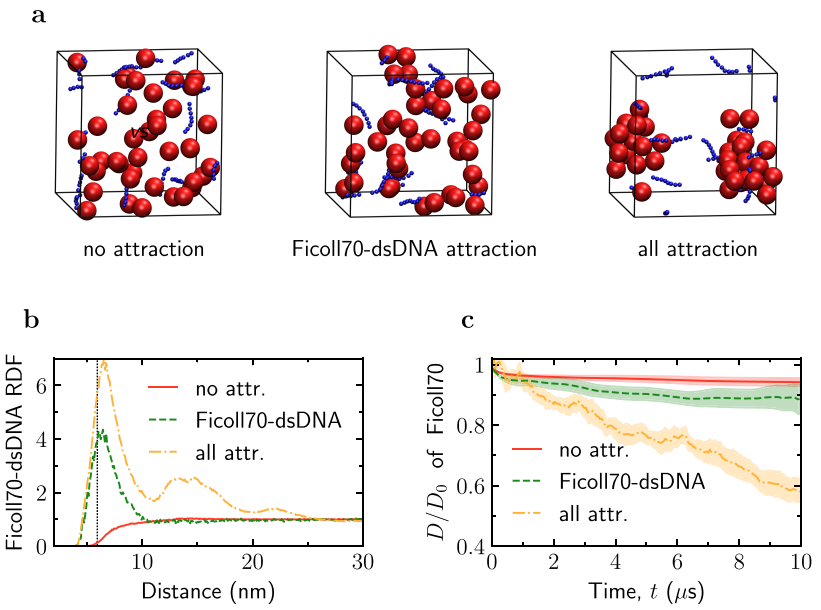

Figure 5. Effect of attraction on macromolecular diffusion from BD simulations. (a) Snapshots from BD simulations for systems with no attraction between the macromolecules, with attraction only between Ficoll70 and dsDNA, and with attractive interactions between all macromolecules. The Lennard−Jones interaction parameter $\epsilon_{LJ} = 0.37$ kcal mol^{-1} was taken from ref 24. (b) Ficoll70−dsDNA radial distribution function (RDF) and the (c) time-dependent diffusion coefficient of Ficoll70 for the three considered systems. D_0 is the diffusion coefficient of Ficoll70 in infinite dilution in water (no crowders). The occupied volume fraction $\phi_{occ} = 5\%$ and the molar fraction of dsDNA $x_{DNA} = 25\%$. The shadowed areas show the uncertainties due to sampling errors.

consistent with the observation that crowding affects rotational motion less significantly than translational motion.[23,33,47]

Effect of Attractive Interactions. Although the shape-induced slowdown of diffusion was significant (Figures 2b and 3d), it was smaller than observed in the experiments (Figure 1b,c). A possible reason is that attractive Lennard−Jones (LJ) interactions were not taken into account in our simulations. To assess the role of such interactions, we have simulated two additional systems, in which attractive interactions were allowed (i) between Ficoll70 and dsDNA and (ii) between all macromolecules. Simulation snapshots together with the corresponding Ficoll70−dsDNA radial distribution functions (RDFs) are shown in Figure 5a,b (see also Figure S6). For the system with no attractive interactions, the RDF increases slowly from the soft-core region and approaches unity at large separations, exhibiting no maximum in between. In the system in which all macromolecules interacted with the attractive LJ potential, the macromolecules formed large clusters, leading to a drastic slowdown of the diffusion coefficient. A similarly strong slowdown due to clustering has been reported earlier.[24]

In the case when there is attraction only between dsDNA and Ficoll70 (as a tracer), a well-defined single maximum develops at separations roughly corresponding to the sum of the radii of the tracer and dsDNA's bead (vertical dotted line in Figure 5b), manifesting the formation of dsDNA-tracer "pairs". This is reflected in the diffusive behavior of the tracer, which slows down about 2 times more strongly than in the system with no attractive interactions (from 5% to more than 10% slowdown, Figure 5c).

We have not found experimental or simulation data on streptavidin−dsDNA interactions, but it can be assumed that millimolar concentrations of dsDNA cause at least transient binding between a streptavidin tracer and dsDNA. In contrast to dsDNA, Ficoll exhibits minimal chemical interactions with protein molecules. It thus seems reasonable to assume that streptavidin−dsDNA interact more strongly with each other than Ficoll and streptavidin do. In the FCS study (Figure 1), diffusion of streptavidin was measured in a mixture of Ficoll70 and dsDNA, with the streptavidin concentration in the low nanomolar regime. Thus, even a small amount of dsDNA would be sufficient for one or more dsDNA molecules to attach to streptavidin and form a (transient) complex.

We note that streptavidin acquires a local negative charge ($3e$) due to labeling and may thus seem to repel from dsDNA. However, this additional electrostatic repulsion was relatively weak in our systems because electrostatic interactions were strongly screened with the Debye screening length of about 2.3 nm. In addition, since the charge is localized on the streptavidin surface, a dsDNA can reorient itself to avoid direct contact with this charge when forming a complex. While this may affect the probability of forming a complex, we expect the overall effect to be small and thus neglect it in our reasoning below. Nevertheless, it will be interesting to study such effects in future work.

To estimate from simulations that how transient tracer−dsDNA binding influences the tracer diffusion, we proceeded as follows. By analyzing the distance matrices and taking the first maximum of the RDF as a separation criterion, we calculated that the tracer (which was Ficoll70 in our simulations) was in close contact with dsDNA beads $f \approx 0.085$ fraction of simulation time; for comparison, in the system without attraction $f \approx 0.003$. Assuming that dsDNA−tracer pairing is the only additional source of diffusion slowdown, the diffusion coefficient can be estimated as

$$D = fD_{bound} + (1 - f)D_{free} \quad (4)$$

where D_{bound} is the diffusion coefficient of a tracer−dsDNA complex and D_{free} is the diffusion coefficient of the tracer in the same system but without attractive interactions (we assume here that attraction does not influence the tracer diffusion other than

https://dx.doi.org/10.1021/acs.jpcb.0c04846
J. Phys. Chem. B 2020, 124, 7537−7543

via mediating the tracer−crowder binding). Since D and D_{free} are known from the simulations, eq 4 allowed us to estimate D_{bound}. We found $D_{bound}/D_0 \approx 0.35 \pm 0.29$ (large inaccuracy is due to large sampling errors), which covers the experimentally observed slowdown of streptavidin in the dsDNA solution (ϕ_{occ} = 5% in Figure 1). This reasoning is also consistent with our experimental observation that diffusion of streptavidin in a Ficoll70−dsDNA mixture was slowed down significantly already at a low molar fraction of dsDNA (25%), while a further increase of the dsDNA concentration led to comparatively moderate effects (Figure 1c).

CONCLUSIONS

Our study shows that solely due to larger excluded volumes (e.g., 30% vs 70% for 5% occupied volume fraction, Figure 2d), nonspherical macromolecules can cause a few-fold stronger slowdown of diffusion than spherical crowders (Figure 2b), which are often used to mimic the cytoplasm in simulations[13,24−28] and in experiments.[10,13,16,21,34] The attraction between a tracer and crowders may lead to the formation of transient complexes and further slowdown of diffusion (Figure 5). These two effects have likely combined to give rise to the stunning 60% slowdown observed at just 5% occupied volume fraction in the case of cylindrically shaped dsDNA crowders and a streptavidin tracer (Figure 1). This shows that high volume fractions are not needed to significantly reduce diffusion and suggests that models based on spherical macromolecules and steric and hydrodynamic interactions might be too simplistic to properly describe diffusion inside living cells.

With BD simulations we also found that rotational diffusion of dsDNA is less influenced by the crowder shape than its translational diffusion (Figure 4). This is in line with the fact that rotations are generally less affected by crowding than translational motion.[23,33,47]

Recent studies show that nonspherical crowders, as compared with spherical ones, can reduce the closure time of polymer chains[48] and significantly affect protein folding.[3] To better understand the role of the diversity of macromolecular shapes in cellular life, it will be interesting to study how crowders' shapes influence metabolic reactions, chemical equilibria, and other biologically relevant processes.

ASSOCIATED CONTENT

Supporting Information

The Supporting Information is available free of charge at https://pubs.acs.org/doi/10.1021/acs.jpcb.0c04846.

Details of Brownian dynamics simulations and trajectory analysis, the dsDNA model for simulations, the excluded volume calculations and Monte Carlo simulations, experimental details and data analysis, and supplementary plots and tables (PDF)

AUTHOR INFORMATION

Corresponding Authors

Jörg Fitter − *I. Physikalisches Institut (IA), AG Biophysik, RWTH Aachen University, 52074 Aachen, Germany; Institut für Biologische Informationsprozesse (IBI-6), Forschungszentrum Jülich, 52425 Jülich, Germany;* orcid.org/0000-0002-4503-2079; Email: fitter@physik.rwth-aachen.de.

Svyatoslav Kondrat − *Department of Complex Systems, Institute of Physical Chemistry, Polish Academy of Sciences, 01-224 Warsaw, Poland; Max-Planck-Institut für Intelligente Systeme, 70569 Stuttgart, Germany; Institut für Theoretische Physik IV, Universität Stuttgart, 70569 Stuttgart, Germany;* orcid.org/0000-0003-4448-0686; Email: skondrat@ichf.edu.pl, svyatoslav.kondrat@gmail.com.

Authors

Tomasz Skóra − *Department of Complex Systems, Institute of Physical Chemistry, Polish Academy of Sciences, 01-224 Warsaw, Poland;* orcid.org/0000-0003-4394-4928

Farzaneh Vaghefikia − *I. Physikalisches Institut (IA), AG Biophysik, RWTH Aachen University, 52074 Aachen, Germany*

Complete contact information is available at: https://pubs.acs.org/10.1021/acs.jpcb.0c04846

Notes

The authors declare no competing financial interest.

ACKNOWLEDGMENTS

This work was supported by NCN (grant no. 2017/25/B/ST3/02456) to S.K. and T.S. The authors thank PLGrid for providing computational resources. We are grateful to our Bachelor student Christian Justus (RWTH) for helping with the FCS measurements. We thank Matthias Weiss (University of Bayreuth) and Gerhard Gompper (Forschungszentrum Jülich) for the interest in our work and insightful discussions during the Workshop "Soft matter at interfaces 2020" in Ringberg (February 23−26, 2020).

REFERENCES

(1) Fulton, A. B. How crowded is the cytoplasm. *Cell* **1982**, *30*, 345−347.

(2) Zimmerman, S. B.; Trach, S. O. Estimation of macromolecule concentrations and excluded volume effects for the cytoplasm of *Escherichia coli*. *J. Mol. Biol.* **1991**, *222*, 599−620.

(3) Gomez, D.; Huber, K.; Klumpp, S. On Protein Folding in Crowded Conditions. *J. Phys. Chem. Lett.* **2019**, *10*, 7650−7656.

(4) Ellis, R. J. Macromolecular crowding: Obvious but underappreciated. *Trends Biochem. Sci.* **2001**, *26*, 597−604.

(5) Tabaka, M.; Kalwarczyk, T.; Holyst, R. Quantitative influence of macromolecular crowding on gene regulation kinetics. *Nucleic Acids Res.* **2014**, *42*, 727−738.

(6) Rohwer, J. M.; Postma, P. W.; Kholodenko, B. N.; Westerhoff, H. V. Implications of macromolecular crowding for signal transduction and metabolite channeling. *Proc. Natl. Acad. Sci. U.S.A.* **1998**, *95*, 10547−10552.

(7) Pastor, I.; Pitulice, L.; Balcells, C.; Vilaseca, E.; Madurga, S.; Isvoran, A.; Cascante, M.; Mas, F. Effect of crowding by Dextrans in enzymatic reactions. *Biophys. Chem.* **2014**, *185*, 8−13.

(8) Kuzmak, A.; Carmali, S.; von Lieres, E.; Russell, A. J.; Kondrat, S. Can enzyme proximity accelerate cascade reactions. *Sci. Rep.* **2019**, *9*, No. 455.

(9) Wojcieszyn, J. W.; Schlegel, R. A.; Wu, E.-S.; Jacobson, K. A. Diffusion of injected macromolecules within the cytoplasm of living cells. *Proc. Natl. Acad. Sci. U.S.A.* **1981**, *78*, 4407−4410.

(10) Dauty, E.; Verkman, A. S. Molecular crowding reduces to a similar extent the diffusion of small solutes and macromolecules: Measurement by fluorescence correlation spectroscopy. *J. Mol. Recognit.* **2004**, *17*, 441−447.

(11) Dix, J. A.; Verkman, A. Crowding Effects on Diffusion in Solutions and Cells. *Annu. Rev. Biophys.* **2008**, *37*, 247−263.

(12) Feig, M.; Yu, I.; Wang, P. H.; Nawrocki, G.; Sugita, Y. Crowding in Cellular Environments at an Atomistic Level from Computer Simulations. *J. Phys. Chem. B* **2017**, *121*, 8009−8025.

(13) Kondrat, S. *Physics and Modelling of Intracellular Diffusion*; Forschungszentrum Juelich Publishing, 2018; Chapter D1; Vol. *158*, pp 1−16.

(14) Collins, M.; Mohajerani, F.; Ghosh, S.; Guha, R.; Lee, T.-H.; Butler, P. J.; Sen, A.; Velegol, D. Nonuniform Crowding Enhances Transport. *ACS Nano* **2019**, *13*, 8946−8956.
(15) Grimaldo, M.; Lopez, H.; Beck, C.; Roosen-Runge, F.; Moulin, M.; Devos, J. M.; Laux, V.; Härtlein, M.; Da Vela, S.; Schweins, R.; et al. Protein Short-Time Diffusion in a Naturally Crowded Environment. *J. Phys. Chem. Lett.* **2019**, *10*, 1709−1715.
(16) Junker, N. O.; Vaghefikia, F.; Albarghash, A.; Höfig, H.; Kempe, D.; Walter, J.; Otten, J.; Pohl, M.; Katranidis, A.; Wiegand, S.; et al. The Impact of Molecular Crowding on Translational Mobility and Conformational Properties of Biological Macromolecules. *J. Phys. Chem. B* **2019**, *123*, 4477−4486.
(17) Nawrocki, G.; Karaboga, A.; Sugita, Y.; Feig, M. Effect of protein-protein interactions and solvent viscosity on the rotational diffusion of proteins in crowded environments. *Phys. Chem. Chem. Phys.* **2019**, *21*, 876−883.
(18) Soh, S.; Byrska, M.; Kandere-Grzybowska, K.; Grzybowski, B. A. Reaction-diffusion systems in intracellular molecular transport and control. *Angew. Chem., Int. Ed.* **2010**, *49*, 4170−4198.
(19) Schavemaker, P. E.; Boersma, A. J.; Poolman, B. How important is protein diffusion in prokaryotes. *Front. Mol. Biosci.* **2018**, *5*, No. 93.
(20) Weiss, M.; Elsner, M.; Kartberg, F.; Nilsson, T. Anomalous subdiffusion is a measure for cytoplasmic crowding in living cells. *Biophys. J.* **2004**, *87*, 3518−3524.
(21) Banks, D. S.; Fradin, C. Anomalous diffusion of proteins due to molecular crowding. *Biophys. J.* **2005**, *89*, 2960−2971.
(22) Szymanski, J.; Weiss, M. Elucidating the origin of anomalous diffusion in crowded fluids. *Phys. Rev. Lett.* **2009**, *103*, No. 038102.
(23) McGuffee, S. R.; Elcock, A. H. Diffusion, crowding & protein stability in a dynamic molecular model of the bacterial cytoplasm. *PLoS Comput. Biol.* **2010**, *6*, No. e1000694.
(24) Ando, T.; Skolnick, J. Crowding and hydrodynamic interactions likely dominate in vivo macromolecular motion. *Proc. Natl. Acad. Sci. U.S.A.* **2010**, *107*, 18457−18462.
(25) Blanco, P. M.; Garcés, J. L.; Madurga, S.; Mas, F. Macromolecular diffusion in crowded media beyond the hard-sphere model. *Soft Matter* **2018**, *14*, 3105−3114.
(26) Frembgen-Kesner, T.; Elcock, A. H. Computer simulations of the bacterial cytoplasm. *Biophys. Rev.* **2013**, *5*, 109−119.
(27) Kondrat, S.; Zimmermann, O.; Wiechert, W.; Lieres, E. V. The effect of composition on diffusion of macromolecules in a crowded environment. *Phys. Biol.* **2015**, *12*, No. 046003.
(28) Miyaguchi, T. Reduction of self-diffusion coefficient in a coarse-grained model of cytoplasm. *Phys. Rev. Res.* **2020**, *2*, No. 013279.
(29) Goodsell, D. S. A look inside the living cell. *Am. Sci.* **1992**, *80*, 457−465.
(30) Długosz, M.; Antosiewicz, J. M. Transient effects of excluded volume interactions on the translational diffusion of hydrodynamically anisotropic molecules. *J. Chem. Theory Comput.* **2014**, *10*, 2583−2590.
(31) Myung, J. S.; Roosen-Runge, F.; Winkler, R. G.; Gompper, G.; Schurtenberger, P.; Stradner, A. Weak Shape Anisotropy Leads to a Nonmonotonic Contribution to Crowding, Impacting Protein Dynamics under Physiologically Relevant Conditions. *J. Phys. Chem. B* **2018**, *122*, 12396−12402.
(32) Shin, J.; Cherstvy, A. G.; Metzler, R. Self-subdiffusion in solutions of star-shaped crowders: Non-monotonic effects of inter-particle interactions. *New J. Phys.* **2015**, *17*, No. 113028.
(33) Balbo, J.; Mereghetti, P.; Herten, D. P.; Wade, R. C. The shape of protein crowders is a major determinant of protein diffusion. *Biophys. J.* **2013**, *104*, 1576−1584.
(34) Kalwarczyk, T.; Ziebacz, N.; Bielejewska, A.; Zaboklicka, E.; Koynov, K.; Szymański, J.; Wilk, A.; Patkowski, A.; Gapiński, J.; Butt, H. J.; et al. Comparative analysis of viscosity of complex liquids and cytoplasm of mammalian cells at the nanoscale. *Nano Lett.* **2011**, *11*, 2157−2163.
(35) Długosz, M.; Zieliński, P.; Trylska, J. Brownian dynamics simulations on CPU and GPU with BD_BOX. *J. Comput. Chem.* **2011**, *32*, 2734−2744.
(36) Henderson, D.; Duh, D.-M.; Chu, X.; Wasan, D. An expression for the dispersion force between colloidal particles. *J. Colloid Interface Sci.* **1997**, *185*, 265−268.
(37) Hamaker, H. C. The London-van der Waals attraction between spherical particles. *Physica* **1937**, *4*, 1058−1072.
(38) Israelachvili, J. N. *Intermolecular and Surface Forces*; Elsevier, 2015.
(39) Rotne, J.; Prager, S. Variational treatment of hydrodynamic interaction in polymers. *J. Chem. Phys.* **1969**, *50*, 4831−4837.
(40) Yamakawa, H. Transport properties of polymer chains in dilute solution: hydrodynamic interaction. *J. Chem. Phys.* **1970**, *53*, 436−443.
(41) Zuk, P. J.; Wajnryb, E.; Mizerski, K. A.; Szymczak, P. Rotne−Prager−Yamakawa approximation for different-sized particles in application to macromolecular bead models. *J. Fluid Mech.* **2014**, *741*, R5.
(42) Smith, E. R.; Snook, I. K.; Van Megen, W. Hydrodynamic interactions in Brownian dynamics: I. Periodic boundary conditions for computer simulations. *Physica A* **1987**, *143*, 441−467.
(43) Iniesta, A.; de la Torre, J. A second-order algorithm for the simulation of the Brownian dynamics of macromolecular models. *J. Chem. Phys.* **1990**, *92*, 2015−2018.
(44) Cichocki, B.; Rubin, M.; Niedzwiecka, A.; Szymczak, P. Diffusion coefficients of elastic macromolecules. *J. Fluid Mech.* **2019**, *878*, R3.
(45) Lauffer, M. A. Theory of Diffusion in Gels. *Biophys. J.* **1961**, *1*, 205−213.
(46) Novak, I. L.; Kraikivski, P.; Slepchenko, B. M. Diffusion in cytoplasm: Effects of excluded volume due to internal membranes and cytoskeletal structures. *Biophys. J.* **2009**, *97*, 758−767.
(47) Swaminathan, R.; Hoang, C. P.; Verkman, A. S. Photobleaching recovery and anisotropy decay of green fluorescent protein GFP-S65T in solution and cells: Cytoplasmic viscosity probed by green fluorescent protein translational and rotational diffusion. *Biophys. J.* **1997**, *72*, 1900−1907.
(48) Xia, B. C.; Zhang, D. H.; Wang, J. J.; Yu, W. C. Effects of Shape of Crowders on Dynamics of a Polymer Chain Closure. *Chin. J. Chem. Phys.* **2017**, *30*, 343−347.

https://dx.doi.org/10.1021/acs.jpcb.0c04846
J. Phys. Chem. B 2020, 124, 7537−7543